J Solid State Electrochem (2004) 8: 110–117
DOI 10.1007/s10008-003-0392-x

ORIGINAL PAPER

Gyoung-Ja Lee · Su-Il Pyun · Chang-Hee Kim

Kinetics of double-layer charging/discharging of the activated carbon fiber cloth electrode: effects of pore length distribution and solution resistance

Received: 13 February 2003 / Accepted: 13 April 2003 / Published online: 17 June 2003

Abstract The effects of pore length distribution (PLD) and solution resistance, R_{sol}, on the kinetics of double-layer charging/discharging of the activated carbon fiber cloth electrode (ACFCE) were investigated in a 30 wt% H_2SO_4 solution using nitrogen gas adsorption, a.c. impedance spectroscopy, the current transient technique, and cyclic voltammetry. The impedance spectra of the ACFCE were theoretically calculated based upon the transmission line model in consideration of the pore size distribution (PSD) and the PLD. From comparison of both the experimental and theoretical impedance spectra of the ACFCE, it is suggested that the deviation from the ideal impedance behavior of a cylindrical pore in the experimental impedance spectrum of the ACFCE is mainly ascribed to PLD, rather than to PSD. The cathodic current transients and cyclic voltammograms were theoretically calculated based upon the transmission line model as functions of the standard deviation σ of the PLD and R_{sol}. From the results, it is concluded that ion penetration into the pores is closely related to both σ and R_{sol} during double-layer charging/discharging of the ACFCE, that is, the larger σ and R_{sol}, the lower is the rate capability, thus causing higher retardation of ion penetration into the pores.

Keywords Activated carbon fiber cloth · Pore length distribution · Pore size distribution · Solution resistance · Transmission line model

G.-J. Lee · S.-I. Pyun (✉) · C.-H. Kim
Department of Materials Science and Engineering,
Korea Advanced Institute of Science and Technology,
373-1 Guseong-dong, Yuseong-gu,
Daejeon 305-701, Republic of Korea
E-mail: sipyun@webmail.kaist.ac.kr
Tel.: +82-42-8693319
Fax: +82-42-8693310

Introduction

Over the last two decades, electric double-layer capacitors (EDLCs) have been considered as one of the most attractive energy storage devices because of their high power density, high capacitance, and high charging/discharging rates [1, 2, 3, 4, 5]. Highly porous activated carbons are widely used as the electrode materials in EDLCs, due to such advantageous features as high surface area, good electrical conductivity, and adequate corrosion resistance. Unfortunately, however, these advantages have proven not to be enough to realize the high power application. That is, much of the active surface is accessible only through the cumulative resistance of the electrolyte inside the pore. Therefore, the porous structure of the activated carbon becomes one of the most important factors for the high double-layer charging/discharging rates [3].

In previous work [6, 7] from our laboratory it has been reported that the kinetics of double-layer charging/discharging is crucially affected by pore size distribution (PSD) of the activated carbon electrodes. Song et al. [8] revealed that the non-ideal impedance behavior of the porous electrode is attributable to the PSD, i.e. a wider distribution of the pore size leads to more frequency dispersion in the impedance spectra. Momma et al. [2] also reported that the activated carbon fiber electrode significantly deviated from the ideal impedance behavior of a cylindrical pore in the impedance spectrum; nevertheless, it is well known that it exhibits a quite narrow PSD.

It is generally accepted that the porous carbon electrodes widely used in EDLCs have both types of distributed characteristics: one from the PSD and the other from the pore length distribution (PLD). Furthermore, the solution resistance, R_{sol}, between the reference electrode and the front surface of the porous electrode affects ion penetration into the pores [9]. This implies that the PLD and R_{sol} also influence the kinetics of the double-layer charging/discharging process of the EDLCs.

In this respect, the present work aims at investigating the effects of the PLD and R_{sol} on the kinetics of double-layer charging/discharging of the activated carbon fiber cloth electrode (ACFCE). For this purpose, a.c. impedance spectrum, potentiostatic current transient, and cyclic voltammogram (CV) were measured on the ACFCE. In addition, the potentiostatic current transients and the CVs were theoretically calculated based upon the transmission line model in consideration of the PLD and R_{sol} as functions of the standard deviation σ of the PLD and R_{sol}.

Experimental

The ACFCE was prepared by heat treatment of the commercially activated carbon fiber cloth (CH700-10: thickness = 0.55 mm, Kuraray Chemicals, Japan) in an electric furnace at 1000 °C for 2 h in an atmosphere of argon gas in order to remove the surface acidic functional groups (SAFGs) formed on the ACFCE.

The PSD and the surface area of the ACFCE were determined by a gas adsorption analyzer (Micrometrics ASAP2010) with the help of nitrogen gas adsorption at 77 K after degassing the ACFCE at 200 °C for 12 h. The total Brunauer, Emmett, and Teller (BET) surface area and PSD were calculated by using isotherms of nitrogen gas from the BET equation [10] and the Horvath–Kawazoe equation [11], respectively.

A three-electrode electrochemical cell was employed for the electrochemical measurements. A platinum gauze and a saturated calomel electrode (SCE) were used as the counter electrode and the reference electrode, respectively. Prior to the electrochemical measurements, the ACFCE was vacuum wetted, and the aqueous solution of 30 wt% H_2SO_4 was deaerated by bubbling with purified argon gas for 24 h. The apparent area of the ACFCE exposed to the electrolyte amounted to 1 cm^2.

The a.c. impedance was measured using a frequency response analyzer (Solartron, SI 1255 FRA) in conjunction with a potentiostat (Solartron, SI 1287 ECI) with a 5 mV a.c. signal superimposed on an applied potential of 0.1 V (vs. SCE) over the frequency range of 10^{-2} to 10^3 Hz. The potentiostatic current transient was measured on the ACFCE by application of a potential drop from 0.1 to 0.08 V (vs. SCE) by using the potentiostat (Solartron, SI 1287 ECI). The cyclic voltammetry measurements were performed in the potential range of 0–0.5 V (vs. SCE) with scan rates of 20 and 40 mV s^{-1} using an EG&G PARC model 263A potentiostat/galvanostat.

Results and discussion

Gas adsorption analysis

Figure 1a and Fig. 1b plot the cumulative pore volume, V, and the differential pore volume, dV/dr, against the pore radius, r, for the ACFCE obtained by the Horvath–Kawazoe equation, respectively. The value of V sharply increased below an r value of 1.2 nm and reached a constant value above an r value of about 3 nm. The total pore volume, V_{tot}, was measured as 0.6 cm^3 g^{-1}.

The PSD was concentrated in the range from 0.8 to 1.2 nm with an average pore radius, r_{ave}, of 1.0 nm, as shown in Fig. 1b. Since the sizes of nitrogen gas at 77 K and hydrated ions in aqueous electrolyte are comparable with each other, the pores accessible to nitrogen gas at 77 K are also available to aqueous electrolyte [12, 13]. Therefore, the parameters obtained by the nitrogen gas adsorption method are acceptable to be used in the analyses of the electrochemical results in aqueous electrolyte. The total BET surface area calculated using isotherms of nitrogen gas from the BET equation was determined to be 1170 m^2 g^{-1}.

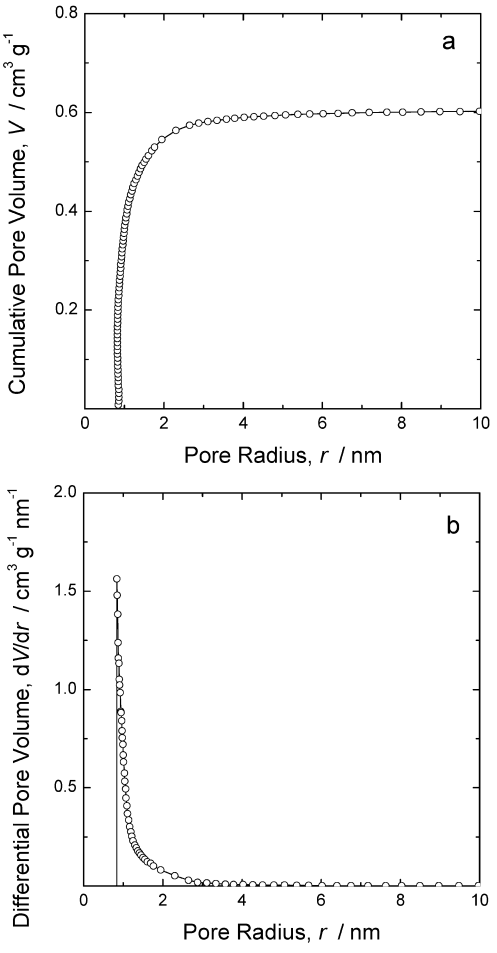

Fig. 1 Plots of **a** cumulative pore volume and **b** differential pore volume against pore radius for the activated carbon fiber cloth electrode (ACFCE), obtained by the Horvath–Kawazoe equation

A.c. impedance analysis

Figure 2 demonstrates the Nyquist plot obtained from the ACFCE in a 30 wt% H_2SO_4 solution (shown as open circles). The impedance measurement was conducted at an applied potential of 0.1 V (vs. SCE), where any faradaic current arising from the oxidation and reduction of the SAFGs or from the decomposition of electrolyte is free [6].

The impedance spectrum measured on the ACFCE consisted of a straight line inclined at a constant phase angle to the real axis at high frequencies and an almost vertical capacitive line at low frequencies. The straight inclined line at high frequencies is attributable to the semi-infinite ion migration through the pores. The capacitive line at low frequencies is due to the accumulation of ions at the bottom of the pores.

It is generally known [14, 15] that the shape of the pores comprising the activated carbon fiber is cylindrical and homogeneous throughout the bulk of the fiber. Moreover, it can be assumed that the surface of the pores is homogeneous, because the SAFGs formed on the ACFCE, which give rise to the surface inhomogeneity, are removed by the heat treatment. In view of these circumstances, de Levie's transmission line model [16, 17, 18] was adopted for theoretical calculation of the impedance spectrum.

When the interfacial impedance of a pore is represented by a double-layer capacitance, the impedance of a pore, Z_o, based upon de Levie's transmission line model is expressed by:

$$Z_o = (1-j)\left(\frac{R}{2\omega C}\right)^{1/2} \coth\left[(1+j)\left(\frac{\omega RC}{2}\right)^{1/2} l_p\right] \quad (1)$$

with:

$$R = \frac{1}{k\pi r^2} \text{ and } C = C_d 2\pi r \quad (2)$$

where R is the resistance of the electrolyte inside a pore per unit pore length (Ω cm^{-1}); C is the double-layer capacitance of the electrode/electrolyte interface per unit pore length (F cm^{-1}); ω is the angular frequency (rad s^{-1}); l_p is the pore length (cm); k is the conductivity of the electrolyte (Ω^{-1} cm^{-1}); and C_d represents the specific double-layer capacitance per unit area (Ω cm^{-2}). If n pores of a porous electrode with the same r and l_p are located in parallel, the total impedance of the electrode, Z_{tot}, is given by:

$$Z_{tot} = \frac{Z_o}{n} \quad (3)$$

It is well known that the impedance spectrum of a cylindrical pore has a phase angle of 45° in value at high frequencies and a phase angle of 90° in value at low frequencies. However, it is seen from Fig. 2 that the phase angle of the impedance spectrum measured on the ACFCE was larger than 45° in value at high frequencies and smaller than 90° in value at low frequencies. Song et al. [8] reported that such non-ideal impedance behavior of the porous electrode composed of cylindrical pores is ascribable to the PSD. In this regard, we first considered the PSD of the ACFCE as the origin of the deviation from the ideal impedance behavior of a cylindrical pore in the impedance spectrum.

Considering the PSD, Z_{tot} is given by:

$$\frac{1}{Z_{tot}} = \int_{-\infty}^{\infty} \frac{1}{Z_o} f(r)\mathrm{d}r \approx \sum_i \frac{1}{Z_{o,i}} f_i \Delta r_i \equiv \sum_i \frac{1}{Z_{o,i}} n_i \quad (4)$$

where $f(r)$ and $f(r)\mathrm{d}r$ represent the distribution density function of the pore size and the number of the pores between r and $r+\mathrm{d}r$, respectively. The C_d of the ACFCE was determined to be 1.2 F cm^{-2} at the lowest frequency, i.e. 10^{-2} Hz in the impedance spectrum.

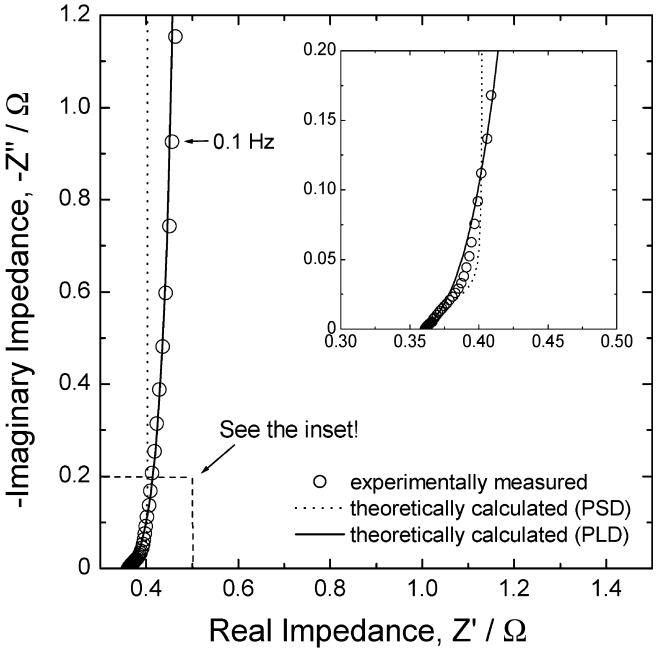

Fig. 2 Nyquist plot of the impedance spectrum experimentally measured on the ACFCE at an applied potential of 0.1 V (vs. SCE) in a 30 wt% H_2SO_4 solution. *Dotted* and *solid lines* represent the impedance spectra theoretically calculated based upon the transmission line model in consideration of the pore size distribution (PSD) and the pore length distribution (PLD), respectively

The l_p was fixed at the average pore length, l_{ave}, which is obtained [19] from:

$$l_{ave} = \sqrt{R_{tot} V_{tot} mk} \quad (5)$$

where R_{tot} is the total resistance of the electrolyte inside pores (Ω) and m is the mass of the ACFCE (g). Here, R_{tot} is three times the value determined by extrapolation of the low-frequency branch toward the real impedance axis [16, 17]. By taking the values $R_{tot} = 0.12\ \Omega$, $V_{tot} = 0.6$ cm^3 g^{-1}, $m = 0.014$ g, and $k = 0.85\ \Omega^{-1}$ cm^{-1}, l_{ave} was found to be 0.029 cm. The number of pores for a given pore radius, n_i, was obtained from division of the whole pore volume by the single pore volume for a given pore radius, $\pi r_i^2 l_{ave}$, in Fig. 1.

The dotted line in Fig. 2 represents the impedance spectrum theoretically calculated from Eq. 4 based upon the transmission line model in consideration of the PSD. It is noted that the experimentally measured impedance spectrum for the ACFCE did not accord well in value and shape with the theoretically calculated one. The theoretically calculated impedance spectrum showed the almost ideal impedance behavior of a cylindrical pore.

Remembering that the PSD of the ACFCE is quite narrow, it is not surprising that the PSD of the ACFCE hardly influences the deviation from the ideal impedance behavior of a cylindrical pore in the impedance spectrum. Therefore, from now on, we will calculate theoretically the impedance spectrum based upon the transmission line model in consideration of the PLD in

order to clarify the origin of the non-ideal impedance behavior of the ACFCE.

It is assumed [8, 22] that the pore length l_p takes a log-normal distribution, $f(x)$, given by:

$$f(x) = \frac{V_{tot}}{\pi r^2 l_p}\frac{1}{\sqrt{2\pi}\sigma}\exp\left[-\frac{1}{2}\left(\frac{x-\mu}{\sigma}\right)^2\right] \quad (6)$$

with:

$$x = \ln(l_p/l_o) \quad (7)$$

where x denotes the natural logarithm of l_p divided by an arbitrary unit length l_o to obtain a dimensionless quantity, and μ and σ are the mean value and the standard deviation of the distribution variable x, respectively.

On substituting:

$$y = \frac{x-\mu}{\sigma} \quad (8)$$

into Eq. 6, we obtain:

$$f(y) = \frac{V_{tot}}{\pi r^2 l_p}\frac{1}{\sqrt{2\pi}}\exp\left(-\frac{1}{2}y^2\right) \quad (9)$$

Hence, Z_{tot} becomes:

$$\frac{1}{Z_{tot}} = \int_{-\infty}^{\infty}\frac{1}{Z_o}f(y)\mathrm{d}y = \int_{-\infty}^{\infty}\frac{1}{Z_o}\frac{V_{tot}}{\pi r^2 l_p}\frac{1}{\sqrt{2\pi}}\exp\left(-\frac{1}{2}y^2\right)\mathrm{d}y \quad (10)$$

Here, r is set at the r_{ave} value and the PLD satisfies the following condition:

$$\int_{-\infty}^{\infty}\frac{1}{\sqrt{2\pi}}\exp\left(-\frac{1}{2}y^2\right)\mathrm{d}y = 1 \quad (11)$$

The theoretically calculated impedance spectrum in consideration of the PLD is exhibited in Fig. 2, shown as a solid line. From the comparison of the impedance spectrum experimentally measured with that theoretically calculated, one finds that the impedance spectrum calculated at $\mu = -3.52$ and $\sigma = 0.7$ fits best to that experimentally measured. The chi-squared (χ^2) value, representing the square of the standard deviation between the experimental spectrum and the calculated one, was determined to be 6.5×10^{-3}. It should be emphasized that the experimentally measured and theoretically calculated impedance spectra coincided fairly well with each other, indicating that the PLD crucially influences the deviation from the ideal impedance behavior of a cylindrical pore in value and shape.

Kinetic approach to the double-layer charging/discharging of the ACFCE

In the presence of solution resistance R_{sol} (Ω) between the reference electrode (RE) and the working electrode (WE), the current of a pore, $I(t)$, at a given potential step is expressed [20] as:

$$I(t) = \frac{2\Delta E}{R_{sol}}\sum_{n=1}^{\infty}\frac{\Lambda}{\Lambda^2+\Lambda+m_n^2}\exp\left(-m_n^2 krt\Big/2C_d l_p^2\right) \quad (12)$$

with:

$$\Lambda = \frac{R_p}{R_{sol}} \quad \text{and} \quad R_{sol} = \frac{l_s}{k\pi r^2} \quad (13)$$

where ΔE is the potential step (V); R_p is the resistance of the electrolyte inside a pore (Ω); l_s is the distance between the RE and the WE (cm); and m_n represents the nth positive root of $(m\tan m - \Lambda) = 0$.

When the PLD is considered together with R_{sol}, the total current, $I_{tot}(t)$, is written as:

$$\begin{aligned} I_{tot}(t) &= \int I(t)f(y)\mathrm{d}y \\ &= \int \tfrac{2\Delta E}{R_{sol}}\sum_{n=1}^{\infty}\tfrac{\Lambda}{\Lambda^2+\Lambda+m_n^2}\exp\left(-m_n^2 krt\Big/2C_d l_p^2\right) \\ &\quad \times \tfrac{V_{tot}}{\pi r^2 l_p}\tfrac{1}{\sqrt{2\pi}}\exp\left(-\tfrac{1}{2}y^2\right)\mathrm{d}y \end{aligned} \quad (14)$$

where $f(y)$ and $f(y)\mathrm{d}y$ represent the density distribution of the pore length and the number of the pores between y and $y+\mathrm{d}y$, respectively. The value of l_s was measured to be 0.12 cm and hence the resulting R_{sol} was calculated to be 4.4×10^{12} Ω. All other parameters for the theoretical calculation of $I_{tot}(t)$ are shared with those of the calculated impedance spectrum.

The cathodic current transient theoretically calculated based upon the transmission line model in consideration of the PLD and R_{sol} is displayed in Fig. 3 (shown as a solid line), along with that experimentally measured (shown as open circles). The theoretical current transient was in good agreement with the experimentally measured one. From the quantitative coincidence of the theoretical current transient with the experimental one, it is reasonable to say that both the PLD and R_{sol} crucially influence the current transient in value and shape.

Under the circumstances, we investigated the effect of the PLD and R_{sol} on the kinetics of the double-layer charging/discharging of the ACFCE. For this purpose, the cathodic current transients and CVs were theoretically calculated based upon the transmission line model as functions of σ of the PLD and R_{sol}. To simplify the theoretical calculation, we assumed that the cross-sectional area of the ACFCE was the same and hence that the n value was constant irrespective of σ. In addition, for any σ, the PLD should satisfy the condition of Eq. 11 with μ fixed in order to take into consideration all the pores comprising the ACFCE.

Figure 4a illustrates on a logarithmic scale the cathodic current transients theoretically calculated from Eq. 14 based upon the transmission line model as a function of σ of the PLD. The initial current levels were equal in value irrespective of σ. For $\sigma = 0.1$, the current transient exhibited a slow decay, followed by a steep decay. As σ increased, the slope of the current transient

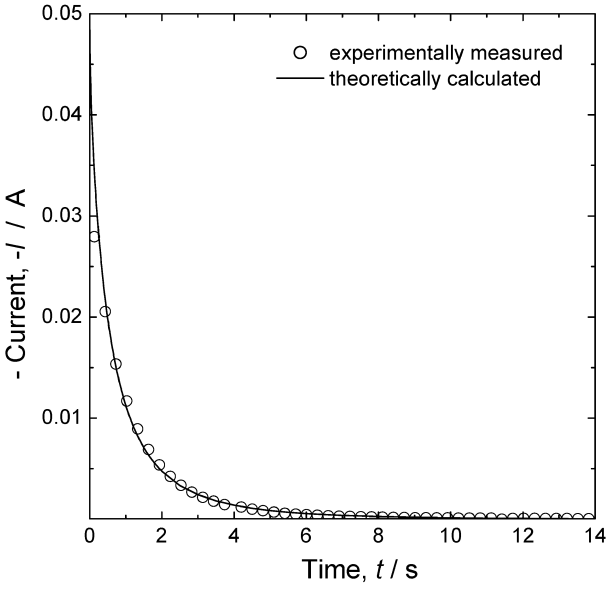

Fig. 3 The cathodic current transient experimentally measured on the ACFCE in a 30 wt% H_2SO_4 solution by dropping the applied potential from 0.1 to 0.08 V (vs. SCE). The *solid line* represents the theoretically calculated cathodic current transient

was steeper in earlier time and the time to reach the constant current of 5×10^{-5} A was more prolonged.

In order to clearly observe the change in shape of the current transient, we introduced "the derivative" of the logarithmic cathodic current transient with respect to logarithmic time, as shown in Fig. 4b. It is noticeable that the plots of the derivatives versus logarithmic time consist of two regions: region I where the absolute values of the derivatives increased with increasing σ, and region II where they decreased with increasing σ. This means that as σ increases, the current decays more rapidly with time in region I, whereas it decays more slowly with time in region II.

During the cathodic current transient, as the time goes on, the ions penetrate into the pores and then reach the bottom of the pores. If the radii of all the pores are the same, the larger the pore length, the longer is the time to reach the bottom of the pores. In region I, the rapid current decay with increasing σ is due to the dominant contribution of pores with a smaller length. On the other hand, in region II the slow current decay and more prolonged time to reach the constant current of 5×10^{-5} A with increasing σ is due to the dominant contribution of pores with a larger length.

Figure 5a envisages on a logarithmic scale the cathodic current transients theoretically calculated from Eq. 14 based upon the transmission line model as a function of R_{sol}. As R_{sol} increased, the initial current level decreased in value and the time to reach the constant current of 5×10^{-5} A was significantly prolonged. Also, it seemed that the current decayed more slowly as R_{sol} increased.

The derivatives of the logarithmic cathodic current transients theoretically calculated from Eq. 14 based upon the transmission line model as a function of R_{sol}

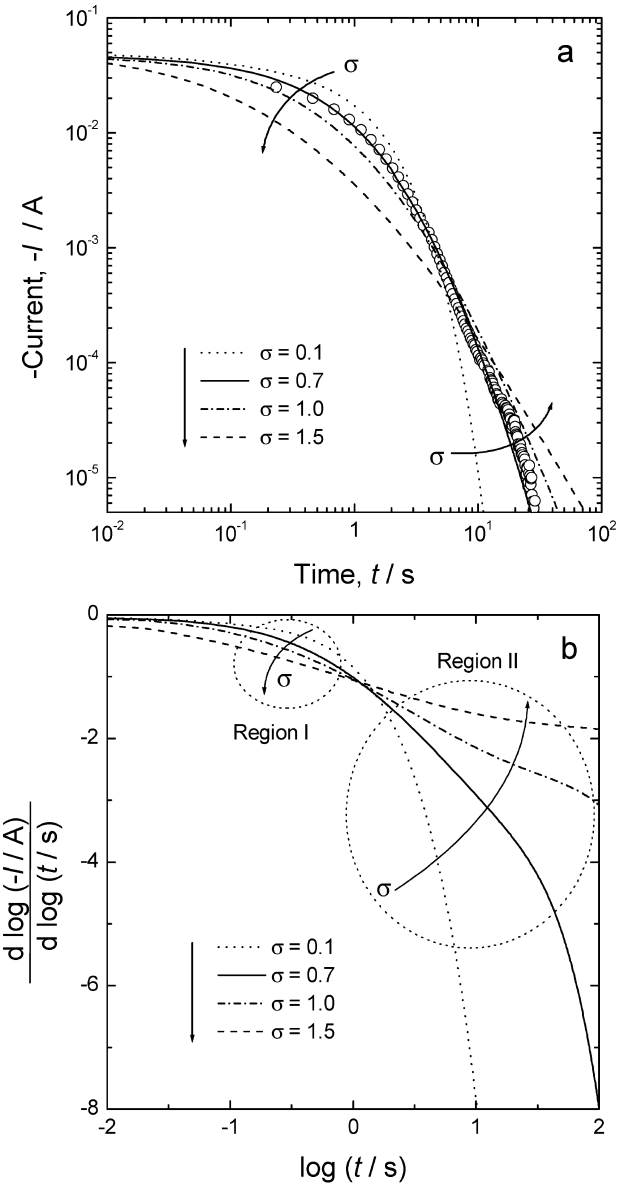

Fig. 4 a The cathodic current transients on a logarithmic scale and **b** the derivatives of the logarithmic cathodic current transients theoretically calculated from Eq. 14 based upon the transmission line model as a function of standard deviation σ of the PLD. The *open circles* in **a** represent the cathodic current transient experimentally measured on the ACFCE

are presented in Fig. 5b. The absolute values of the derivatives monotonically decreased with increasing R_{sol}. This indicates that, as R_{sol} increases, the current decays more slowly over the whole time during double-layer charging of the ACFCE, which is ascribed to the higher retardation of ion penetration into the pores.

Now, we extend the kinetic investigation of double-layer charging/discharging of the ACFCE to the case of potential scanning. During the potential scan with a scan rate v, in consideration of R_{sol}, the $I(t)$ is written [21] as:

$$I(t) = \alpha v C_d 2\pi r l_p; \qquad \alpha = \beta_1 - \beta_2 \tag{15}$$

with:

$$\beta_1 = 1 - \sum_{n=1}^{\infty} \frac{2\Lambda^2}{m_n^2[\Lambda^2 + \Lambda + m_n^2]} \exp\left(-m_n^2 krt \Big/ 2C_d l_p^2\right) \quad (16)$$

$$\beta_2 = \sum_{n=1}^{\infty} \left(\frac{\Lambda^2 + m_n^2}{\Lambda^2 + \Lambda + m_n^2}\right) \exp\left(-m_n^2 krt \Big/ 2C_d l_p^2\right) \left(\frac{2}{m_n^2}\right) \sin^2 m_n \quad (17)$$

Considering the PLD, $I_{tot}(t)$ is given by:

$$I_{tot}(t) = \int I(t) f(y) \mathrm{d}y$$

$$= \int (\beta_1 - \beta_2) v C_d 2\pi r l_p \frac{V_{tot}}{\pi r^2 l_p} \frac{1}{\sqrt{2\pi}} \exp\left(-\tfrac{1}{2} y^2\right) \mathrm{d}y \quad (18)$$

Figure 6 demonstrates the CVs obtained from the ACFCE at scan rates of 20 and 40 mV s^{-1}. The CVs were recorded in the potential range between 0 and 0.5 V (vs. SCE), where no electrolyte decomposition occurs. The experimental CVs (shown as open circles) were in good accordance with the theoretical ones. It is well known that the CVs for the ideal double-layer capacitor, where the time constant is zero, are characterized by a perfectly rectangular-shaped profile [21]. However, as seen in Fig. 6, the CV profiles for the ACFCE at 20 and 40 mV s^{-1} appreciably deviated from a rectangular shape.

Let us compare the deviation of the CV profiles from the ideal double-layer capacitor for the ACFCE with various σ and R_{sol}. At infinite time, the $I_{tot}(t)$ reaches the following steady-state current:

$$I_{tot}(\infty) = \int v C_d 2\pi r l_p \frac{V_{tot}}{\pi r^2 l_p} \frac{1}{\sqrt{2\pi}} \exp\left(-\frac{1}{2} y^2\right) \mathrm{d}y \quad (19)$$

The $I_{tot}(t)$ values were normalized with respect to $I_{tot}(\infty)$, as shown in Fig. 7. Figure 7a and Fig. 7b exhibit the plots of the reduced current against the applied potential theoretically calculated from Eq. 18 based upon the transmission line model as functions of σ of the PLD and R_{sol}, respectively, at a scan rate of 20 mV s^{-1}. It is noticeable that the deviation from the ideal double-layer capacitor increased with increasing both σ and R_{sol}. In particular, the reduced current for the ACFCE with larger σ and R_{sol} never reached unity, i.e. the steady-state current, in the potential range under investigation.

Here, we quantitatively estimated the rate capability γ as the quotient of the reduced charge for the ACFCE divided by the reduced charge for the ideal double-layer capacitor, which is given as:

$$\gamma = \frac{Q_{real}}{Q_{ideal}} = \frac{\int \left\{\frac{I_{tot}(t)}{I_{tot}(\infty)}\right\}_{real} \mathrm{d}t}{\int \left\{\frac{I_{tot}(t)}{I_{tot}(\infty)}\right\}_{ideal} \mathrm{d}t}$$

$$\approx \frac{\int \left\{\frac{\int (\beta_1 - \beta_2) v C_d 2\pi r l_p \times f(y) \mathrm{d}y}{\int v C_d 2\pi r l_p \times f(y) \mathrm{d}y}\right\}_{real} \mathrm{d}t}{\int \left\{\frac{\int (\beta_1 - \beta_2) v C_d 2\pi r l_p \times f(y) \mathrm{d}y}{\int v C_d 2\pi r l_p \times f(y) \mathrm{d}y}\right\}_{ideal} \mathrm{d}t} \quad (20)$$

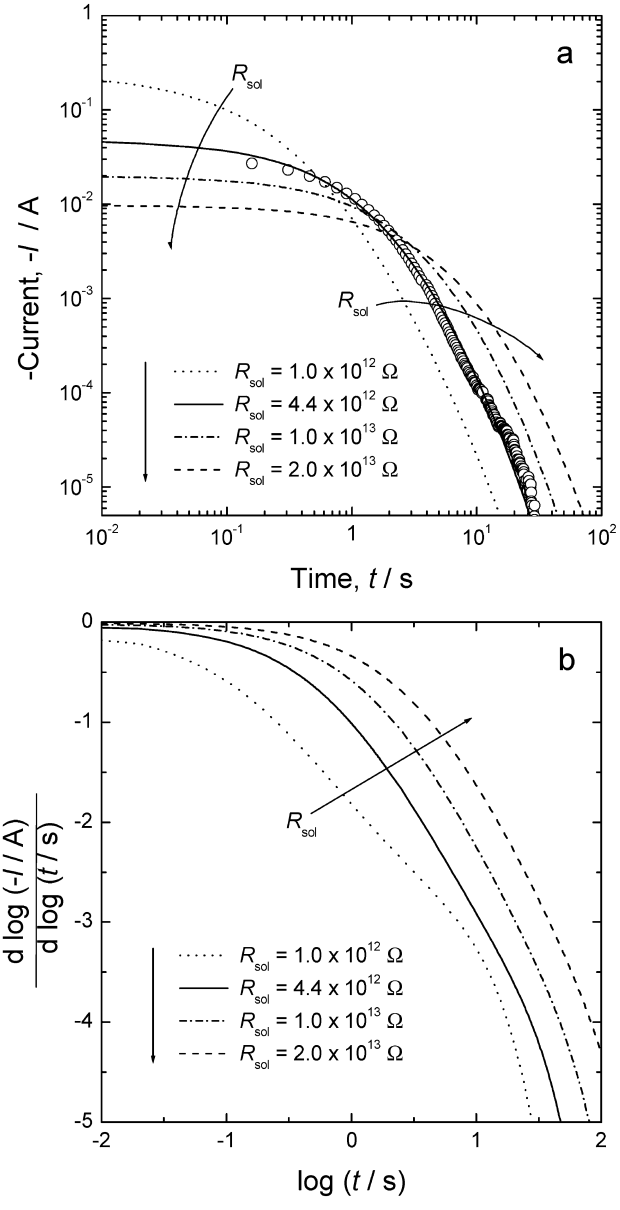

Fig. 5 **a** The cathodic current transients on a logarithmic scale and **b** the derivatives of the logarithmic cathodic current transients theoretically calculated from Eq. 14 based upon the transmission line model as a function of R_{sol}. The *open circles* in **a** represent the cathodic current transient experimentally measured on the ACFCE

where Q_{real} is the charge for the ACFCE and Q_{ideal} is the charge for the ideal double-layer capacitor.

The rate capabilities γ increased with increasing σ and R_{sol}, as summarized in Table 1. This indicates that the ion penetration into the pores during double-layer charging/discharging is more impeded with increasing values of both σ and R_{sol}. From these results, it is concluded that ion penetration into the pores is closely related to both σ and R_{sol} during double-layer charging/discharging of the ACFCE, that is, the larger σ and R_{sol}, the lower is the rate capability γ.

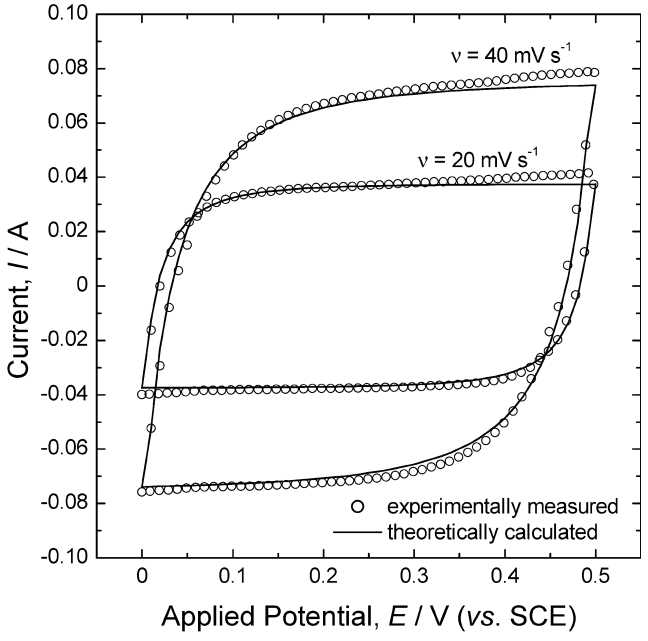

Fig. 6 Cyclic voltammograms experimentally measured on the ACFCE with scan rates of 20 and 40 mV s^{-1} in a 30 wt% H_2SO_4 solution. The *solid lines* represent the theoretically calculated CVs

Conclusions

The present work involves the effects of the PLD and R_{sol} on the kinetics of double-layer charging/discharging of the ACFCE by analyses of the a.c. impedance spectra, cathodic current transients, and CVs. From the results experimentally measured and theoretically calculated, the following conclusions are drawn:

1. The Nyquist plot of the impedance spectrum experimentally measured on the carbon electrode hardly followed the ideal impedance behavior of a cylindrical pore. From the comparison of the impedance spectra experimentally measured and theoretically calculated based upon the transmission line model in consideration of the PSD and the PLD of the ACFCE, it is concluded that such non-ideal impedance behavior of the ACFCE is mainly due to the PLD rather than to the PSD.
2. The cathodic current transient experimentally measured on the ACFCE coincided well with that theoretically calculated based upon the transmission line model in consideration of the PLD and R_{sol}. From the results of the derivatives of the logarithmic cathodic current transients theoretically calculated as a function of σ of the PLD, it was found that as σ increased, the current decayed more rapidly with time due to the dominant contribution of pores with a smaller length in region I, whereas the current decayed more slowly with time due to the dominant contribution of pores with a larger length in region II. Besides, as R_{sol} increased, the theoretically calculated cathodic current monotonically decayed more slowly

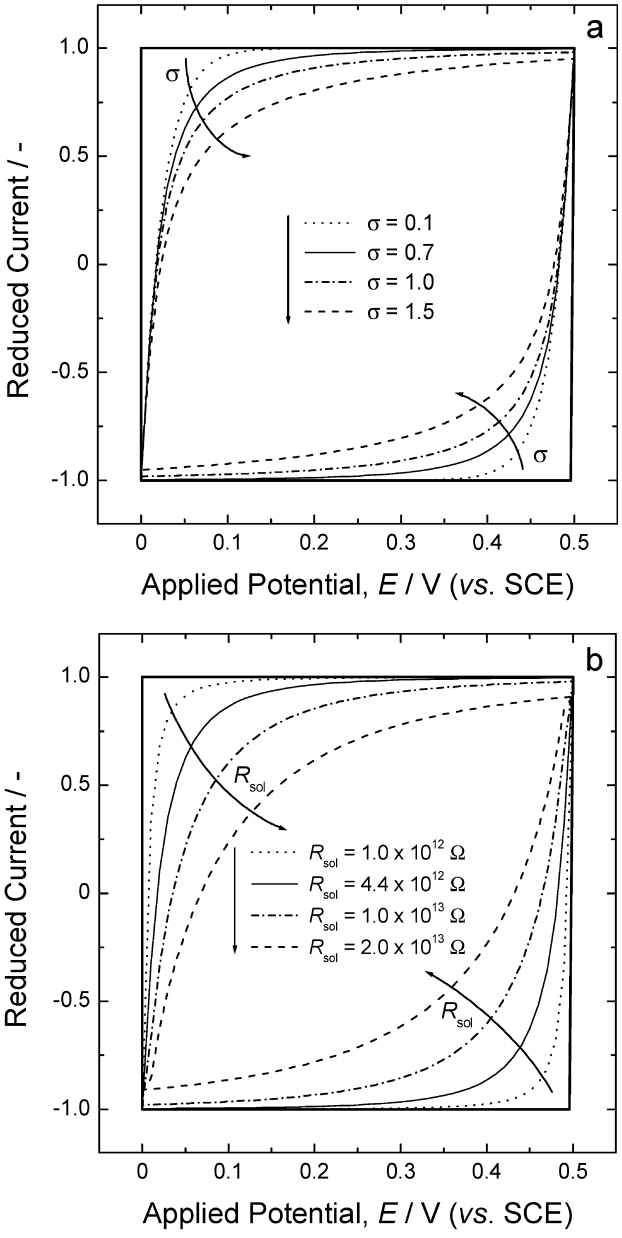

Fig. 7 Plots of the reduced current against the applied potential theoretically calculated based upon the transmission line model as functions of **a** σ of the PLD and **b** of R_{sol} at a scan rate of 20 mV s^{-1}. The *solid bold line* denotes the ideal double-layer capacitor where the time constant is zero

Table 1 The rate capabilities γ calculated by dividing the reduced charge for the ACFCE by the reduced charge for the ideal double-layer capacitor

Standard deviation, σ	Rate capability, γ	Solution resistance, R_{sol} (Ω)	Rate capability, γ
0.1	0.90	1.0×10^{12}	0.94
0.7	0.86	4.4×10^{12}	0.86
1.0	0.82	1.0×10^{13}	0.74
1.5	0.73	2.0×10^{13}	0.52

with time due to the higher retardation of ion penetration into the pores.

3. The CVs experimentally measured on the carbon electrode were in fair agreement with those theoretically calculated based upon the transmission line model in consideration of the PLD and R_{sol}. The rate capability γ, defined as the quotient of the reduced charge for the ACFCE divided by the reduced charge for the ideal double layer capacitor, decreased with increasing σ and R_{sol}. This suggests that ion penetration into the pores during double-layer charging/discharging is more impeded as σ and R_{sol} increase.

Acknowledgements This work was supported by a grant no. R01-2000-000-00240-0 from Korea Science & Engineering Foundation. This work was partly supported by the Brain Korea 21 project.

References

1. Ishikawa M, Sakamoto A, Morita M, Matsuda Y, Isida K (1996) J Power Sources 60:233
2. Momma T, Liu X, Osaka T, Ushio Y, Sawada Y (1996) J Power Sources 60:249
3. Qu D, Shi H (1998) J Power Sources 74:99
4. Nakagawa H, Shudo A, Miura K (2000) J Electrochem Soc 147:38
5. Weng TC, Teng H (2001) J Electrochem Soc 148:A368
6. Kim CH, Pyun SI, Shin HC (2002) J Electrochem Soc 149:A93
7. Pyun SI, Kim CH, Kim SW, Kim JH (2002) J New Mater Electrochem Syst 5:289
8. Song HK, Lee YH, Dao Le H (1999) Electrochim Acta 44: 3513
9. Jin X, Zhuang L, Lu J (2001) J Electroanal Chem 519:137
10. Brunauer S, Emmett PH, Teller E (1938) J Am Chem Soc 60:309
11. Horvath G, Kawazoe K (1983) J Chem Eng Jpn 16:470
12. Soffer A, Folman M (1972) J Electroanal Chem 38:25
13. Shi H (1996) Electrochim Acta 41:1633
14. Oshida K, Kogiso K, Takeuchi K, Kobayashi S, Endo M, Dresselhaus MS, Dresselhaus G (1995) J Mater Res 5:2507
15. Daley MA, Tandon D, Economy J, Hippo EJ (1996) Carbon 34:1191
16. de Levie R (1964) Electrochim Acta 9:1231
17. de Levie R (1965) Electrochim Acta 10:113
18. de Levie R (1967) Advances in electrochemistry and electrochemical engineering, vol VI. John Wiley & Sons, New York, p 329
19. Candy JP, Fouilloux P (1980) Electrochim Acta 26:1029
20. Posey FA, Morozumi T (1966) J Electrochem Soc 113:176
21. Austin LG, Gagnon EG (1973) J Electrochem Soc 120:251
22. Diard JP, Le Gorrec B, Montella C (2001) J Electroanal Chem 499:67